This is the peer reviewed version of the following article: S. Mattiello, A. Monguzzi, J. Pedrini, M. Sassi, C. Villa, Y. Torrente, R. Marotta, F. Meinardi and L. Beverina, Adv. Funct. Mater., 2016, 26, 8447–8454., which has been published in final form at [http://doi.wiley.com/10.1002/adfm.201603303]. This article may be used for non-commercial purposes in accordance with Wiley Terms and Conditions for Use of Self-Archived Versions."

Article type: Full Paper

Self-assembled dual dye-doped nanosized micelles for high-contrast up-conversion bioimaging.

By *Sara Mattiello, Angelo Monguzzi, Jacopo Pedrini, Mauro Sassi, Chiara Villa, Yvan Torrente, Roberto Marotta, Francesco Meinardi, and Luca Beverina**

[*] Prof. L. Beverina, Prof. F. Meinardi, Dr. A. Monguzzi, Dr. M. Sassi, Dr. J. Pedrini, Dr. S. Mattiello
Dipartimento di Scienza dei Materiali
Università degli Studi Milano-Bicocca
via R. Cozzi 55, 20125 Milan , Italy
E-mail: luca.beverina@unimib.it

Dr. C. Villa, Prof. Y. Torrente
Stem Cell Laboratory, Department of Pathophysiology and Transplantation,
Università degli Studi di Milano, Fondazione IRCCS Ca' Granda Ospedale Maggiore Policlinico, Centro Dino Ferrari,
via F. Sforza 35, 20122 Milan, Italy

Dr. R. Marotta
Istituto Italiano di Tecnologia. Via Morego 30, 16163 Genova, Italy

Keywords: photon up-conversion, anti-Stokes imaging, self-assembled superstructures, multicomponent nanomaterials, high biocompatibility

Sensitized triplet-triplet annihilation based photon up-conversion (TTA-UC) greatly improves the scope and applicability of fluorescence bioimaging by enabling anti-Stokes detection at low powers, thus eliminating the background autofluorescence and limiting the potential damage of the living tissues. Here we present a facile, one-step protocol to prepare dual dye doped, TTA-UC active nanomicelles starting from the commercially available surfactant Kolliphor EL®, a component of several FDA approved preparations. These nanosized micelles show an unprecedented up-conversion yield of 6.5% under 0.1 W cm^{-2} excitation intensity in an aqueous, non-deareated dispersion. The supramolecular architecture obtained preserves the embedded dyes from oxygen quenching, allowing satisfactory anti-Stokes fluorescence imaging of 3T3 stem cells. This is the first example of efficient multicomponent up-converters prepared by using highly biocompatible materials approved by the international

authority, paving the way for the development of new complex and multifunctional materials for advanced theranostics.

1. Introduction

Fluorescence imaging is the most common approach used on biological specimens for visual diagnostics. [1-4] However, even if this technique is very well established, its application on human living patients is still unpractical. Living tissues strongly absorb at the UV-Vis excitation wavelengths required by most of the available and affordable fluorescent probes. [5] As a consequence, practical applications require the use of high intensity sources, with two important consequences: an increased scattering of the excitation light and a stronger background autofluorescence from tissues, which significantly reduce the signal-to-noise ratio of the optical detection, resulting in low-contrast images. Moreover, an intense excitation light greatly increases the potential damage of the tissues under investigation, thereby making harmful an otherwise non-invasive technique.

Many of the most advanced researches in this field aim at overcoming this critical issue. As depicted in Fig. 1a, a possible solution is the use of materials showing anti-Stokes photoluminescence, namely the emission of photons at higher energy than the absorbed ones.[6] This effect is known as photon up-conversion (UC), and it is commonly achieved through nonlinear optical phenomena like the second harmonic generation (SHG) or the two-photon absorption (TPA). By exploiting this peculiar emission is thus possible to eliminate the autofluorescence background, present only at energies lower than the excitation, with a gain in the image contrast enabling the use of low power, innocuous light sources.

The field of anti-Stokes fluorescence imaging was traditionally dominated by inorganic crystals doped with luminescent lanthanide ions and by organolanthanide

complexes, where the UC scheme requires the sequential absorption of two or more photons exciting the metastable states of the emitting ions. [7-10] The anti-Stokes imaging enforced by lanthanide enables the use of infrared light excitation, matching the transparency widows of the biological tissue, but, due to the small UC cross section of the exploited lanthanide electronic transitions, it requires the use of extremely intense excitation sources.[6] The same consideration is valid for TPA materials, where the up-converted light is

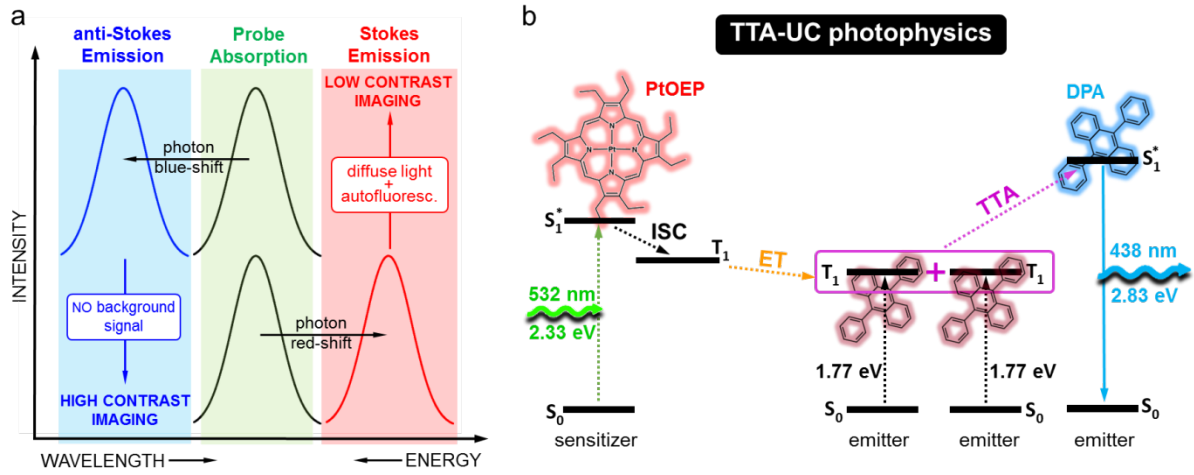

Figure 1. (a) Outline of Stokes and anti-Stokes photoluminescence properties related to the fluorescence imaging application. (b) Photophysics of the TTA-UC process using PtOEP as sensitizer and DPA as emitter. The dotted arrows indicate radiationless transitions. Upon absorption of a green photon, a sensitizer molecule is excited to its first singlet state that efficiently undergoes intersystem crossing (ISC) into the triplet state. If efficient triplet-triplet energy transfer (ET) occurs, the emitter dark triplets are populated before the radiative recombination of sensitizers. Subsequently, the annihilation of two colliding emitter triplets (TTA) generates one high energy, fluorescent emitter in the excited singlet state, from which the blue UC emission occurs.

generated by the simultaneous absorption of two photons. Such approaches were successfully validated over the years for both *in vitro* and *in vivo* applications. Unfortunately, in both cases the required excitation power densities are typically in the order of MW cm^{-2}. [11]

Conversely, the UC based on sensitized triplet-triplet annihilation (TTA-UC), recently proposed as efficient photon managing technique for solar applications, can be observed using excitation power densities of few mW cm^{-2}. [8,11-14] The TTA-UC is a stepwise process which exploits the annihilation of optically dark, metastable triplets of an emitter, indirectly populated from proper sensitizers *via* energy transfer, to produce high-energy singlets, from

which the up-converted emission originates. As detailed in Fig. 1b, the TTA-UC requires a pair of selected chromophores with suitable electronic properties. Here, we used the Pt octaethylporphyrin (PtOEP) as sensitizer and the 9-10-diphenylanthracene (DPA) as annihilator/emitter. The PtOEP can be excited to its first singlet excited state by irradiation at 532 nm, which quickly converts to the low-lying triplet via inter system crossing (ISC). If within the lifetime of this latter, the sensitizer collides with a ground state DPA, the two molecules undergo a triplet-triplet energy transfer (ET) resulting in the excitation of the emitter in its first triplet state. Finally, the collision of two emitter triplets leads to the promotion of one of them in the first, fluorescent singlet excited state through TTA. It is worth pointing out that, since the triplets of the dyes usually employed as emitters are long-living states with typical natural lifetime in the range of hundreds of milliseconds and over, the annihilation is exceptionally efficient, resulting in effective UC also at extremely low excitation light intensity. This allowed proving the TTA-UC scheme with a range of molecule pairs operating in different spectral windows in organic solvents. [15-21] UC-light activated drug release was also demonstrated.[16,22,23] The need to extend this phenomenon to water environment and to biological specimen triggered remarkable efforts in the preparation of TTA-UC structures. Among them, active polymeric structures, [24-29] ionogels, [30] liposomes, [23,31,32] different supramolecular approaches, [24-29] oil in water microemulsions, [33-35] dendrimers, [36] micelles[37] and water dispersable nanoparticles[38,39] and nanocapsules[40-46]led to demonstration of the applicability of TTA-UC both *in vitro* and *in vivo*, within the tissue transparency window. [9,10,38,40,42]

Nowadays, the full exploitation of the TTA-UC scheme in bio-related applications remains challenging due to two characteristic features of this process. First, the molecular oxygen is an excellent quencher of triplet states, switching off quickly the TTA-UC process.. This is a very critical requirement as in biological tissues, where the oxygen tension is around 0.5-2.5 kPa, to be compared with its equilibrium value in air of 21 kPa. [47] The TTA-UC is

actually so sensitive that it was recently used in the preparation of oxygen sensing materials having a particularly broad dynamic range. [48] Second, the sensitizer and emitter counterparts need to be in close proximity in order to efficiently undergo short-range interactions such as ET and TTA. The literature reports several approaches to tackle this limit. The encapsulation of the two active molecules within a polymeric shell provided working UC capsules, having dimensions ranging from hundreds of nanometers to microns. [40,43] The step by step assembly of core/shell structures featuring a liquid, or in any case low viscosity core surrounded by a silica shell provides a very elegant approach to solve at the same time both issues, while maintaining the dimensions of the final TTA-UC nanostructure within the nanometric range. [35] Encapsulation in other inorganic matrices like tungsten oxide, in this case for photo catalysis applications, was also demonstrated. [39] The approach is general and versatile, yet somewhat complicated by its multistep nature. Oil in water microemulsions, requiring an organic solvent based inner phase, also offer a viable and general way to prepare colloids displaying efficient TTA-UC in oxygenated environment. [33,34] Very recently Yanai and Kimizuka demonstrated that the synthesis and water phase self-assembly of amphiphilic cationic acceptor molecules with anionic donor (sensitizer) molecules provides an efficient way to address the oxygen quenching issue by a purely supramolecular approach. [25] Finally, Konig et al. demonstrated efficient TTA-UC in large unilamellar vesicles loaded with suitably functionalized diphenylanthracene derivatives as well as both PtOEP and a Ru bipyridine complex. [31] Unfortunately, all of the aforementioned approaches require either the synthesis of specifically designed chromophores, the incorporation of organic solvents or a complex multistep fabrication of appropriate nanovectors, and therefore they can be impractical in many cases.

In this work, we demonstrate an exceedingly simple procedure for the preparation of efficient TTA up-converting nanomicelles (UC-NM) based on the use of the commercially available surfactant Kolliphor EL®. The latter is one of the most commonly employed

emulsifier for water insoluble drugs and is the key excipient of several FDA approved preparations including Paclitaxel® and Miconazole®.[49] Our synthetic protocol enables the synthesis of stable nanomicelles loaded with a proper dye pair for green-to-blue UC, showing an unprecedented UC efficiency of 6.5% for encapsulated materials. The inclusion of the dyes in the micelles preserves the UC performance in oxygenated deionized water as well as in the phosphate-buffered saline (PBS) solution used in biological research. *In vitro* fluorescence imaging experiments on murine fibroblasts (3T3 cell line) confirmed the high biocompatibility of these supramolecular optical probes, therefore providing evidence of the full compatibility with their use as anti-Stokes markers. Moreover, we envisage that the very nature of the assembly protocol we propose, makes possible to include additional payload molecules alongside with the TTA-UC couple. The disappearance of the UC signal due to the nanomicelles wreckage by an external stimulus would thus give a direct and precise indication of when and where the payload is released within the biological specimen.

2. Up-converting nanomicelles preparation.

For this experiment, we selected PtOEP and DPA as a model sensitizer and emitter because they are amongst the most investigated and performing chromophores used for TTA-UC. [44] Fig. 2a sketches the self-assembly strategy followed for the preparation of the UC-NMs aqueous dispersion. In the first step, we prepared a tetrahydrofuran (THF) solution of PtOEP (40 μM) and DPA (4000 μM), in the stoichiometric ratio of 1:100 that is the preferred feeding ratio to observe efficient TTA-UC in solution. [50] To this, we added Kolliphor EL® and 1,2-propanediol under sonication and we maintained the solution in the ultrasound bath for 30 min. All volatiles were evaporated and the oily residue was taken up either with distilled water or with PBS solution to give a UC-NMs stable dispersion with no appreciable haze (see Fig. S1 of the Supporting Information), suggesting the absence of undesired aggregates. A precise

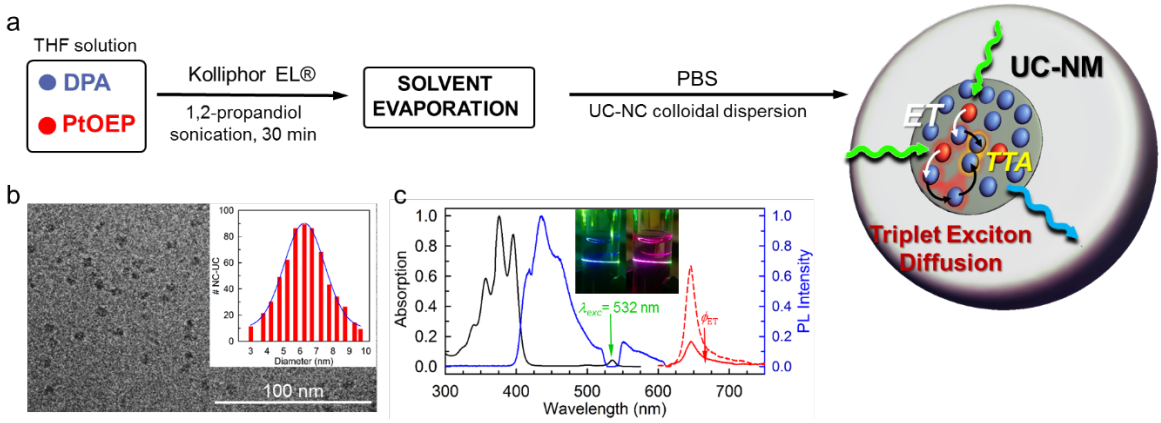

Figure 2. (a) Outline of the UC-NM self-assembly reaction scheme and sketch of the TTA-UC process in a single UC-NM. The up-converted photons are generated thanks to the diffusion (black arrows) and annihilation (TTA) of sensitized dark triplet excitons among the network of acceptors (DPA, blue dots) embedded in the Kolliphor EL® micelles. (b) Cryo-TEM images of UC-NMs loaded with a 100:1 DPA:PtOEP cargo. The inset reports the size distribution of the micellar diameter, peaked at 6.2 nm. (c) Absorption (black line) and photoluminescence (PL, blue line) spectrum of UC-NM under 532 nm laser excitation. The red spectra show the sensitizer (PtOEP, red dots) phosphorescence in presence (solid line) and in absence (dashed line) of the acceptors in the NC. The inset reports a digital picture of the UC-NM dispersion in PBS under 532 excitation with (left) and without (right) a high-pass blue filter.

estimate of the micellar size has been obtained by means of high-resolution Cryo-TEM measurements. This technique has been used in order to avoid the collapse of the micellar structure due to the removal of the dispersing medium. Indeed, the Cryo-TEM images (Fig. 2b) show a series of spherical objects, with a monodisperse diameter distribution peaked at 6.2 nm (inset). These spheroids, given the affinity of DPA and PtOEP with the emulsifier environment and considering their insolubility in the aqueous medium, likely correspond to the amorphous blend of Kolliphor EL®, PtOEP and DPA. Figure S2 of the Supporting Information shows a 3D tomography confirming the micelle nature of the nanoobjects.

In order to verify the presence of both the sensitizer and the emitter chromophores, we recorded the UV-Vis absorption of the dispersion. As reported in Fig. 2c (black line), the UC-NMs spectrum shows the fingerprint absorption peaks of DPA, namely the broad band centred at 380 nm characterized by a well-defined vibronic structure, [51] and of PtOEP, with a weak narrow band centred at 535 nm. [52] These data suggest that both molecules form a stable solution within the Kolliphor EL® matrix, and the UC-NMs spectrum can be precisely

fitted with a convolution of the single dye spectra weighted according to the initial feeding ratio. Consequently, we can assume that the incorporation of DPA and PtOEP is not selective toward one of the two components (Fig. S3). The final demonstration of the successful chromophores loading in the Kolliphor EL® nano-micelles was obtained by recording the photoluminescence (PL) spectrum of the suspension under a laser excitation at 532 nm, matching the PtOEP absorption. Fig. 2c shows that, beside a residual sensitizer phosphorescence at 645 nm due an incomplete ET (red line), we can detect the typical blue emission of DPA (blue line) thanks to the effective UC of the harvested photons. This suggests that the sensitizer and emitter moieties are closely packed in the UC-NMs core, allowing the TTA-UC process through the diffusion of excitons in the dyes framework defined by the micellar volume, without the need of any molecular motion, as sketched in Fig. 2a. To support this view, we performed a simple stochastic simulation of the spatial distribution of DPA molecules in a sphere of 6.2 nm radius, in order to have an approximate estimation the inter-molecular distance. Fig. S4 shows the result of the Montecarlo calculations performed using 56 DPAs per UC-NM (see Supporting Information) and imposing a minimum center-to-center intermolecular distance of 1.0 nm (in accordance with the steric hindrance of the DPA whose molecular radius is 0.45 nm). All the dyes have a nearest-neighbour closer than 1.3 nm and a next-nearest-neighbour closer than 1.5 nm. These values are comparable with the distances at which the exchange interactions are effective, [50] confirming that the excitation energy can migrate *via* exchange-mediated homo-molecular hopping within the ensemble of emitters exploring the micellar volume to experience TTA. The resulting TTA-UC luminescence can be observed also by the naked eyes using a high-pass optical filter, as showed by the digital pictures of the sample (inset of Fig. 2c).

3. Performance analysis of up-converting nanomicelles.

One of the most critical property required to a UC-NM operating in an aqueous medium is a strong ability to shield the chromophores from the environmental oxygen. In order to test this characteristic, we recorded the I_{uc} at different times while leaving the sample in aerated conditions (Fig. 3a). After a 20% drop observed during the first four hours, I_{uc} remains constant up to 10 hours demonstrating the remarkable resistance of the UC-NMs as also observed for other self-assembled structures.[53] The initial decrease of I_{uc} can be simply ascribed to a progressive consumption of the oxygen embedded in the UC-NM during the synthesis.

Dealing with the UC yield (QY_{uc}), in a TTA-UC system, the latter is generally poor at very low excitation intensity I_{exc}, and then it raises by increasing the irradiance of the incident light saturating at its maximum value. Conversely, we measured a noteworthy QY_{uc} of ~6.5% in UC-NM filled with the largest tested concentration of PtOEP and DPA (400 μM, and 4000 μM respectively; in this case we used a 1:10 ratio instead of the 1:100 so far employed due to the limited solubility of DPA in the micelles). Moreover, importantly, the UC-NMs are in the saturation regime for every irradiances above few tens of mW cm^{-2} as it is demonstrated by the linear dependence of the TTA-UC emission vs. I_{exc} at which also corresponds a constant QY_{uc} (Fig. 3b, triangles). Even if such a value is definitely high enough to enable in vitro fluorescence imaging experiments (vide infra), it is lower than that of a liquid solution of PtOEP/DPA with the same concentration in which the QY_{uc} is above 20%.[54] This finding requires some additional comments especially in view of a future optimization of this class of materials.

For an ideal system, the maximum QY_{uc} obtained in the high excitation limit depends only on the sensitizer-to-emitter ET efficiency and on the statistical probability f to obtain a singlet state upon annihilation of two triplets [54]

$$QY_{uc} = 0.5 f \phi_{ET}. \qquad \text{Eq. 1}$$

In Eq. 1 the 0.5 factor simply indicates that two low energy states are required for generating a high energy one, and f is ~1/2. In our system we measured $\phi_{ET} = 55\%$ (see Fig. S7), which implies a QY_{uc} around 12.5%, two times larger than the observed value. In order to justify this discrepancy, and considering that also ϕ_{ET} is not as high as expected for the employed dyes concentrations, we investigated the dyes distribution within the nanomicelles.

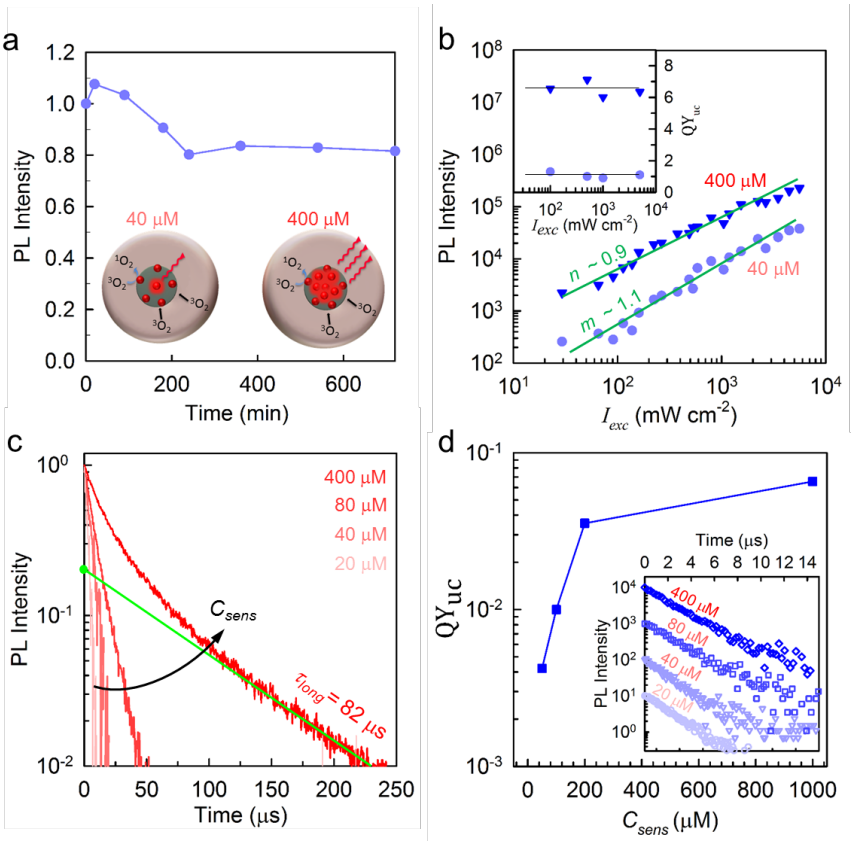

Figure 3. (a) Time dependence of UC emission intensity at 435 nm upon continuous excitation at 532 nm of the as prepared UC-NM sample (PtOEP 40 μM). The inset illustrates the PtOEP molecule distribution in the UC-NM structure with an initial doping concentration of 40 μM and 400 μM. (b) Double logarithmic plot of the UC emission intensity for UC-NM dispersion prepared using 40 μM (dots) and 400 μM (triangles) of the sensitizer PtOEP, as a function of the excitation intensity I_{exc} at 532 nm. The solid straight lines show the fit of the experimental data with a linear function with slope m and n, respectively. The inset show the UC yield QY_{uc} measured at different excitation intensities. (c) Time-resolved PL decay at 645 nm measured for a series of nano-micelles prepared with different PtOEP initial concentrations C_{sens}. (d) QY_{uc}, measured for a series of UC-NM prepared with a fixed DPA initial concentration (4000 μM) as a function of C_{sens}. The inset reports the up-converted light decay at 435 nm for each sample.

To this aim, we prepared two distinct series of UC-NMs. In both of them we varied the sensitizer concentration C_{sens} within the 20 – 400 μM interval. In the first series (series A)

we did not introduce any DPA molecule whiles in the second one (series B) its concentration was 4000 μM. All samples pertaining to series A show the typical red emission of PtOEP (Fig. S6), but with striking differences in their respective luminescence decay dynamics. Fig. 3c reports the time-resolved PL decay recorded at 645 nm as a function of C_{sens}. At the lowest concentration (20 μM), the PL decay is sizeably faster (~3 μs) than PtOEP intrinsic radiative decay time (120 μs). [55] This effect is typical of oxygen quenching, meaning that even though the PtOEP molecules are effectively embedded in the NMs, they do not localize within the dense and hydrophobic core where – according to our data - no oxygen is present, but rather probably at the interface between the oleic core and the polyethyleneglycol hydrophilic shell (inset of Fig. 3a). By increasing the PtOEP concentration its PL lifetime progressively lengthens and becomes clearly non-exponential. In the sample with C_{sens} of 400 μM the PL long-time component is τ_{long} = 82 μs (green solid line). Such a τ_{long} is comparable to the PtOEP decay time usually observed in de-oxygenated organic solvents.[56] This behaviour suggests that the PtOEP molecules preferentially accommodate on, or very close to, the micelle surface where the interaction with the ambient oxygen are not fully prevented. The need to include a higher number of PtOEP molecules per single nanomicelle pushes more PtOEP within the micelle's anoxic core, as showed in the inset of Fig. 3a. The same phenomenology is expected to hold also for the DPA molecules, even if it is not directly detectable because the oxygen sensitive triplet state of this dye are completely dark and no upconversion occurs in the presence of quenching agents. Following this picture, not all the porphyrins are effective as sensitizer for the UC process, but only those inside the NM core can efficiently transfer the excitation to properly included DPA molecules.

Based on the results we obtained with series A samples, we expected a substantial enhancement of the nano-micelles average TTA-UC capabilities by using high C_{sens}. The measurements on series B samples support our general view. Fig. 3d reports the QY_{uc} values

measured as a function of C_{sens} showing that the conversion yield increases from less than 1% in the sample with C_{sens} = 20 μM to 6.5% for the 400 μM sample. These findings suggest that the limited QY_{uc} observed is not related to an inefficient TTA-UC photophysics in the UC-NM environment, but rather on a still not completely optimized distribution of the PtOEP within each single NM structure. This conclusion is strongly supported by the time-resolved data of the TTA-UC emission reported in the inset of Fig. 3d, which show that the dynamic of the upconverted PL is exactly the same regardless C_{sens}, i.e. regardless the overall efficiency of the system. These data proves that, if the incident photons are absorbed by molecules correctly embedded in the NMs structure, the TTA-UC process occurs always in the same, highly efficient way. In contrast, the NMs embedding un-protected dyes are basically inactive as up-converters.

3. In vitro fluorescence imaging with up-conversion nano-micelles.

In order to demonstrate the applicative potential of our NMs, and to verify their stability in biological media, we performed *in vitro* labelling of 3T3 murine fibroblast cell. First of all we proved the absence of any cytotoxic effects induced by the UC-NMs by performing a cell viability assessment by means of Live/Dead staining on cells labelled with increasing nano-micelle concentrations (Fig. S8). The micells do not show any sizeable degradation within the time frame investigated both in the dark and under sunlight exposure (see Fig. S9). The 1:50 dilution of the mother solution resulted the best trade-off between good cell viability, without signs of stress and cell injuries, and UC-NMs concentration providing satisfactory fluorescence imaging. Accordingly, we tested this concentration for further experiments aimed at evaluating the UC-NMs cytocompatibility throughout the time. One of the most frequently reported nanoparticle-associated toxicities is the generation of reactive oxygen species (ROS). ROS are chemically reactive compounds that are formed as a by-product of the cellular oxygen metabolism. However, environmental stress factors such as exposure to

intense light or excessive heating, common consequences of a prolonged irradiation in diagnostic circumstances, can boost the intracellular ROS concentration to cytotoxic levels, causing damage to cell structures and possible cell death. [57] Moreover, oxidative stress induced by the staining with nano-objects can cause further pathophysiological effects including genotoxicity, inflammation, and fibrosis as demonstrated by activation of associated cell signalling pathways. [58] Since oxidative stress is a key determinant of UC-NM-induced injury, it is necessary to characterize the ROS response resulting from the labelling. Cell Titer-Glo viability and ROS evolution assessments have been performed on labelled 3T3 cells throughout 72 hours. Fig. 4a and 4b show the result of the viability and ROS tests,

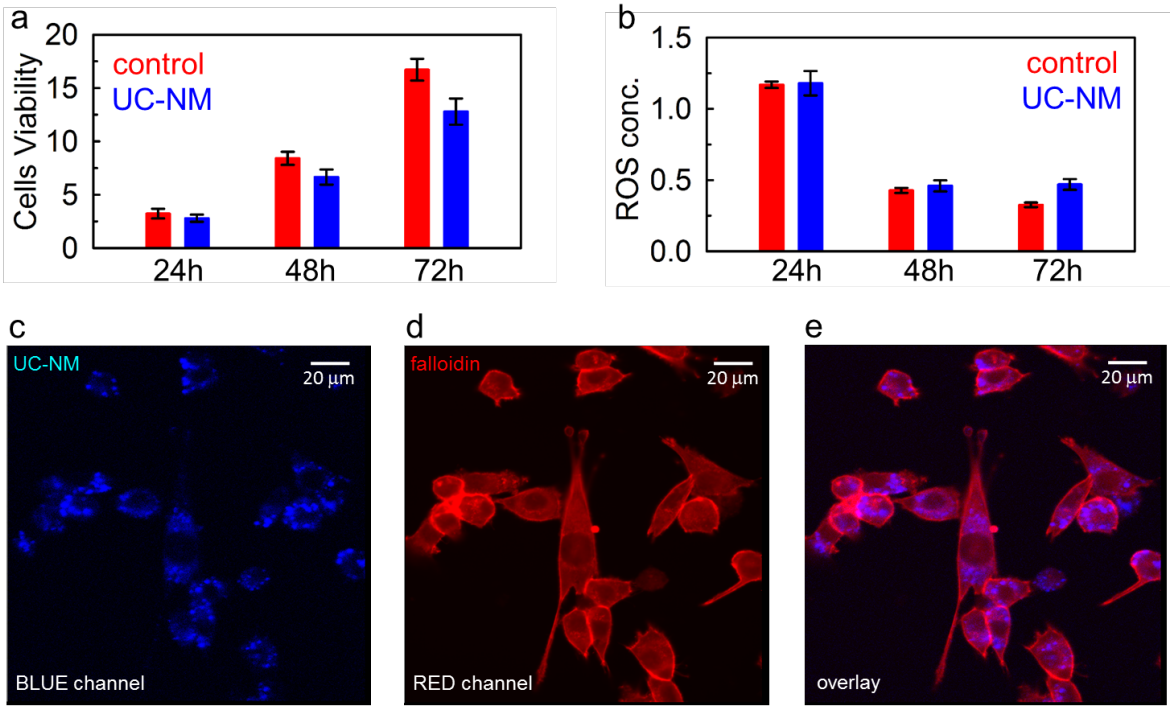

Figure 4. (a) Cell Titer Glow viability test and (b) ROS test on 3T3 cells stained with UC-NMs at 1:50 dilution of the mother solution, monitored at three time points (24h, 48h and 72h, respectively). (c-d) Confocal fluorescence image of 3T3 cell stained with UC-NMs (blue) and phalloidin positive F actin (red) under laser excitation at 532 nm.

respectively. Although the CellTiter-Glo shows a slower proliferation rate for the UC-NM labelled cells compared to the unlabelled control sample (P value <0.005, for 24, 48 and 72 hours), the overall labelled cell viability has been maintained constant through the experiment

course. In the same time, the amount of ROS released from labelled 3T3 cells has been kept on physiological levels, since the ROS production test did not display differences between control and stained samples, confirming the highly biocompatible composition of the UC-NMs.

Finally we proceeded to acquire fluorescence confocal microscope images of paraformaldehyde fixed 3T3 sells stained with UC-NM (blue) and phalloidin positive F actin (red) using a green laser excitation at 532 nm. As shown in Fig. 4, we can clearly observe that the blue UC light is generated in the cytoplasm region mostly around the cell nucleus, as expected for dyes not functionalized with target-specific ligands. In contrast, the phalloidin is a well-known standard dye employed for the specific staining of the cytoskeleton. Therefore, thanks to the overlay of the blue and red channels of the optical detector, we are able to record a nice, high-contrast, dual-channel image of the 3T3 by using the same excitation source (Fig. 4e). This colocalization staining clearly shows that the UC-NMs are effectively internalized by the 3T3 cells, leading to a perinuclear localization and confirming their good stability in the biological medium. This result is the first demonstration of the efficient staining of cells with a TTA-UC based anti-Stokes emitter prepared through such a simple formulation approach employing FDA approved materials. Importantly these results are promising in the perspective of UC-NM applicability as optically active systems for advanced theranostic applications. The observation of UC emission indicates not only that the nanomicelles effectively work as photon up-converters, but it is also an evidence of the structural stability of the micellar structure. As TTA-UC and the corresponding signal would be lost in the case of UC-NMs collapsing, this optical feedback could be used to image the controlled release of water-unsoluble additional payloads embedded within the micells. [2]

4. Conclusion

In summary, we demonstrated a simple and general approach for the preparation of water dispersible, self-assembled nano-micelles loaded with a sensitizer/emitter chromophores pair, which show efficient sensitized up-conversion emission at low excitation power. Thanks to a deep analysis of their optical properties, we were able to optimize the synthesis protocol and obtain nano up-converters with an efficiency of 6.5% in the aqueous, oxygenated environment. The stability of these anti-Stokes emitters in the biological medium in conjunction with suitable biocompatibility enabled us to obtain a multichannel, high-contrast optical imaging of 3T3 cells using a single excitation wavelength. Notably, our material has several advantages with respect to the traditional up-converting systems, such as the low excitation intensity required, limiting the damage to living tissues, and the shielding effect of nano-micelles from oxygen that protect the embedded dyes from quenching and photo-degradation. More importantly, the nano-micelles synthesis is based on a simple formulation with a commercially available surfactant already employed in the formulation of several FDA-approved drugs. To our knowledge, this is the first example of efficient bi-component up-converters prepared by using biocompatible materials approved by the international authority, paving the way for the development of more complex, multicomponent and multifunctional materials for advanced theranostics.

5. Experimental Section.

UC-NM Synthesis. 1,2-propanediol and KH_2PO_4 were purchased from Merck. Na_2HPO_4 was purchased from Alfa Aesar. Distilled water was purchased from Carlo Erba. All the others starting materials were purchased from Sigma-Aldrich. All materials and solvents were used as received.

13.50 mg of DPA and 0.30 mg of PtOEP were dissolved in 10 ml of THF, then 220 mg of 1,2-propanediol/Kolliphor EL® 3:10 v/v mixture were added to 2 ml of the starting solution. The obtained solution was sonicated for 30 minutes in a SONICA® 3200 EP ultrasonic

cleaner, then THF was removed under reduced pressure and the oily residue was taken up either with 15 ml of distilled water or PBS solution.

PBS solution was prepared dissolving 80 g of NaCl, 14.4 g of Na_2HPO_4, 2.4 g of KH_2PO_4 and 2 g of KCl in 1 l of distilled water, and diluting 10 times before use.

UC-NM Structural Analysis. UP-conversion nanoparticles once applied in thin film on glow discharged holey TEM grids were plunge frozen in liquid ethane cooled at liquid nitrogen temperature using a FEI Vitrobot Mark IV semi-automated cryo-plunger. CryoEM projection images and single-axis tilt series were recorded in low dose using a FEI Tecnai G2 F20 Schottky field emission gun transmission electron microscope, equipped with automated cryobox and a Gatan Ultrascan 2kx2k CCD detector. The tilt series were acquired from ± 60° with a tilt angle of 2° at a magnification of 29000 times (pixel size of 0.39 nm) with a total electron dose between 60 and 80 e^-/A^2s. Cryo electron tomograms were calculated and filtered using Imod 3.8.40 (Mastronarde 1997). The 3D model has been obtained using Amira software (FEI Visualization Group).

Photophysical Studies. Absorption spectra have been recorder with a Cary 50 spectrometer in the normal incidence condition using quartz Suprasil cuvettes. CW photoluminescence (PL) signals have been recorded by a nitrogen cooled CCD coupled with a double monochromator Triax-190 (Horiba Jobin-Yvon), with a spectral resolution of 0.5 nm. The recorded spectra have been corrected for the setup optical response. The excitation intensity threshold has been measured by modulating the power of a CW 532 nm doubled Nd:YAG laser Coherent Verdi V10. The excitation laser beam is Gaussian shaped, and the spot diameter containing 90% of the intensity was 340 μm. Shape and spot size have been measured by the knife-edge method. The details of the QY_{uc} measurements are reported as Supporting Information. For time resolved PL measurements we modulated the 532 nm laser

with a TTi TG5011 wavefunctions generator, with a time resolution better than 0.1 μs (5 ns pulse width). Time resolved PL spectra has been detected in photon-counting mode using an ORTEC digital multichannel scaler, with a temporal resolution of 0.1 ns.

Images of UC-NC/phalloidin stained 3T3 cells were acquired with a Nikon C1 confocal microscope coupled with the 532 nm laser focused on the sample with a 60x (1.4 NA) immersion oil objective. The spot size in this configuration is 460 nm. The fluorescence intensity was filtered with blue- and red-pass dichroic mirrors and detected with two photomultiplier tubes with independent gain, in order to record the UC-NM up-converted blue luminescence and the phalloidin red fluorescence, respectively.

Cytotoxicity Test and Cellular Staining.

Cells Culture and Staining Protocols. 3T3 cells (ATCC® CRL-1658™) were thawed and plated on cell culture dish in DMEM high glucose (Gibco) supplemented with 10% FBS (Euroclone) for 48 hours before use. For immunofluorescence experiments, 3T3 cells were detached with 0.25% Trypsin (Gibco), resuspendend in complete medium and plated in 12-well plates at a density of 5x104 cells/well. After 24 hours from seeding, UP-conversion nanoparticles were added to the cells at different concentration of the mother solution (1:10, 1:50, and 1:100). 24 hours after labeling, cell viability was assessed by performing Live Dead fluorescent assay (Thermo Fisher), in accordance with manufacturing protocol. Briefly, Calcein-AM (green-Live) and Ethidium homodimer-1 (red-Death) were diluted 1:1000 in complete medium and incubated for 30 minutes at 37 °C. Cells were then washed twice with Phosphate Buffer Solution (PBS 1x, Gibco) and visualized with an inverted fluorescent miscroscope (Leica). 1:2000 Hoechst counter staining was performed for nuclei visualization. In order to visualize UP-conversion nanoparticles uptake within cells, actin cytoskeleton was labeled with Phalloidin Tetramethylrhodamine B isothiocyanate (TRITC). 3T3 cells were washed with PBS, fixed with 4% formaldehyde solution for 4 minutes, washed twice and

permeabilized by 0.1% Triton X-100 in PBS. After washing in PBS, cells were incubated for 30 minutes with 50µg/ml fluorescent phalloidin conjugated solution; afterward they were extensively washed before visualization. Cells unlabelled were used as control. Since the concentration 1:50 has been shown to maintain both a good cell viability and a high number of detectable nanoparticles, further experiments have considered 1:50 UP-conversion nanoparticles labeled 3T3 cell throughout time (24, 48, 72 hours after labeling).

Cell Viability and ROS Test. For proliferation experiments, cells were seeded in a 96 well plate at 3x103 cells/well density in triplicate (n=3 wells for each time point). Evaluation of Reactive Oxygen Species (ROS) production from cells was performed 24, 48 and 72 hours after 1:50 UP-conversion nanoparticles labelling. ROS-Glo™ H2O2 Assay (Promega) was used, following the producer protocol. Cells treated with 50µM menadione were considered as positive control, while growth medium were reported as negative control. The Non-Lytic protocol was applied for proceeding with additional evaluations on the same cells assessed for ROS production. Specifically, the Cell Titer Glow viability assay (Promega) was performed following the datasheet instruction. The CellTiter-Glo® 3D Cell Viability Assay is a homogeneous method to determine the number of viable cells based on quantitation of the ATP present, which is a marker for the presence of metabolically active cells. For both ROS and Cell Titer Glow assays, relative luminescence units were measured by a plate reader (GloMax Discover, Promega).

Supporting Information

Supporting Information is available from the Wiley Online Library or from the author.

Acknowledgements

L.B. and S.M. gratefully acknowledge Università degli Studi Milano-Bicocca (grant n° 2016-ATESP-0047). A. M. acknowledges support from Università degli Studi Milano-Bicocca

(grant n°2016-ATESP-0052). C.V. and Y.T. acknowledge support from the Associazione Amici del Centro Dino Ferrari and from UNISTEM - Centro di ricerca sulle cellule staminali, Università degli Studi di Milano.

References

[1] J. W. Lichtman, J.-A. Conchello, *Nat. Methods* **2005**, *2*, 910.
[2] K. D. Wegner, N. Hildebrandt, *Chem. Soc. Rev.* **2015**, *44*, 4792.
[3] B. Zhou, B. Shi, D. Jin, X. Liu, *Nature Nanotech* **2015**, *10*, 924.
[4] J. A. Barreto, W. O'Malley, M. Kubeil, B. Graham, H. Stephan, L. Spiccia, *Adv. Mater.* **2011**, *23*, H18.
[5] I. Villa, A. Vedda, I. X. Cantarelli, M. Pedroni, F. Piccinelli, M. Bettinelli, A. Speghini, M. Quintanilla, F. Vetrone, U. Rocha, C. Jacinto, E. Carrasco, F. S. Rodríguez, Á. Juarranz, B. del Rosal, D. H. Ortgies, P. H. Gonzalez, J. G. Solé, D. J. García, *Nano Res.* **2014**, *8*, 649.
[6] J. C. Goldschmidt, S. Fischer, *Adv. Optical Mater.* **2015**, *3*, 510.
[7] F. Wang, *Nat. Mater.* **2011**, *10*, 968.
[8] J. Zhou, Q. Liu, W. Feng, Y. Sun, F. Li, *Chem. Rev.* **2015**, *115*, 395.
[9] W. Feng, X. Zhu, F. Li, *NPG Asia Materials* **2013**, *5*, e75.
[10] L. Zhou, R. Wang, C. Yao, X. Li, C. Wang, X. Zhang, C. Xu, A. Zeng, D. Zhao, F. Zhang, *Nat. Commun.* **2015**, *6*, 1.
[11] C. Ye, L. Zhou, X. Wang, Z. Liang, *Phys. Chem. Chem. Phys.* **2016**, *18*, 10818.
[12] A. Monguzzi, S. M. Borisov, J. Pedrini, I. Klimant, M. Salvalaggio, P. Biagini, F. Melchiorre, C. Lelii, F. Meinardi, *Adv. Funct. Mater.* **2015**, *25*, 5617.
[13] T. F. Schulze, T. W. Schmidt, *Energy Environ. Sci.* **2014**, *8*, 103.
[14] A. Monguzzi, D. Braga, M. Gandini, V. C. Holmberg, D. K. Kim, A. Sahu, D. J. Norris, F. Meinardi, *Nano Lett.* **2014**, *14*, 6644.
[15] K. Xu, J. Zhao, D. Escudero, Z. Mahmood, D. Jacquemin, *J. Phys. Chem. C* **2015**, *119*, 23801.
[16] R. Tao, J. Zhao, F. Zhong, C. Zhang, W. Yang, K. Xu, *Chem. Commun.* **2015**, *51*, 12403.
[17] X. Cui, A. Charaf-Eddin, J. Wang, B. Le Guennic, J. Zhao, D. Jacquemin, *J. Org. Chem.* **2014**, *79*, 2038.
[18] W. Wu, H. Guo, W. Wu, S. Ji, J. Zhao, *J. Org. Chem.* **2011**, *76*, 7056.
[19] V. Yakutkin, S. Aleshchenkov, S. Chernov, T. Miteva, G. Nelles, A. Cheprakov, S. Baluschev, *Chem. Eur. J.* **2008**, *14*, 9846.
[20] T. N. Singh-Rachford, F. N. Castellano, *J. Phys. Chem. A* **2008**, *112*, 3550.
[21] S. Baluschev, V. Yakutkin, T. Miteva, Y. Avlasevich, S. Chernov, S. Aleshchenkov, G. Nelles, A. Cheprakov, A. Yasuda, K. Müllen, G. Wegner, *Angew. Chem. Int. Ed.* **2007**, *46*, 7693.
[22] W. Wang, Q. Liu, C. Zhan, A. Barhoumi, T. Yang, R. G. Wylie, P. A. Armstrong, D. S. Kohane, *Nano Lett.* **2015**, 150709133825001.
[23] S. H. C. Askes, A. Bahreman, S. Bonnet, *Angew. Chem. Int. Ed.* **2013**, *53*, 1029.
[24] C. Ye, J. Wang, X. Wang, P. Ding, Z. Liang, X. Tao, *Phys. Chem. Chem. Phys.* **2016**, *18*, 3430.
[25] H. Kouno, T. Ogawa, S. Amemori, P. Mahato, N. Yanai, N. Kimizuka, *Chem. Sci.*

2016, Advance article, DOI:10.1039/C6SC01047D
[26] T. Gatti, L. Brambilla, M. Tommasini, F. Villafiorita-Monteleone, C. Botta, V. Sarritzu, A. Mura, G. Bongiovanni, M. D. Zoppo, *J. Phys. Chem. C* **2015**, *119*, 17495.
[27] P. Mahato, A. Monguzzi, N. Yanai, T. Yamada, N. Kimizuka, *Nat. Mater.* **2015**, *14*, 924.
[28] J. Zimmermann, R. Mulet, G. D. Scholes, T. Wellens, A. Buchleitner, *J. Chem. Phys.* **2014**, *141*, 184104.
[29] C. Wohnhaas, K. Friedemann, D. Busko, K. Landfester, S. Baluschev, D. Crespy, A. Turshatov, *ACS Macro Lett.* **2013**, *2*, 446.
[30] Y. Murakami, Y. Himuro, T. Ito, R. Morita, K. Niimi, N. Kiyoyanagi, *J. Phys. Chem. B* **2016**, *120*, 748.
[31] M. Poznik, U. Faltermeier, B. Dick, B. König, *RSC Adv.* **2016**, *6*, 41947.
[32] S. H. C. Askes, N. X. S. L. X. P. Mora, R. Harkes, R. I. Koning, B. Koster, T. Schmidt, A. Kros, S. Bonnet, *Chem. Commun.* **2015**, *51*, 9137.
[33] C. Ye, B. Wang, R. Hao, X. Wang, P. Ding, X. Tao, Z. Chen, Z. Liang, Y. Zhou, *J. Mater. Chem. C* **2014**, *2*, 8507.
[34] M. Penconi, P. L. Gentili, G. Massaro, F. Elisei, F. Ortica, *Photochemical & Photobiological Sciences* **2014**, *13*, 48.
[35] Q. Liu, B. Yin, T. Yang, Y. Yang, Z. Shen, P. Yao, F. Li, *J. Am. Chem. Soc.* **2013**, *135*, 5029.
[36] K. Tanaka, K. Inafuku, Y. Chujo, *Chem. Commun.* **2010**, *46*, 4378.
[37] A. Turshatov, D. Busko, S. Baluschev, T. Miteva, K. Landfester, *New J. Phys.* **2011**, *13*, 083035.
[38] O. S. Kwon, H. S. Song, J. Conde, H.-I. Kim, N. Artzi, J.-H. Kim, *ACS Nano* **2016**, *10*, 1512.
[39] J.-H. Kim, J.-H. Kim, *J. Am. Chem. Soc.* **2012**, *134*, 17478.
[40] K. Katta, D. Busko, Y. Avlasevich, R. Muñoz-Espí, S. Baluschev, K. Landfester, *Macromol. Rapid Commun.* **2015**, *36*, 1084.
[41] A. J. Tilley, B. E. Robotham, R. P. Steer, K. P. Ghiggino, *Che. Phys. Lett.* **2015**, *618*, 198.
[42] C. Wohnhaas, V. Mailänder, M. Dröge, M. A. Filatov, D. Busko, Y. Avlasevich, S. Baluschev, T. Miteva, K. Landfester, A. Turshatov, *Macromol. Biosci.* **2013**, *13*, 1422.
[43] J.-H. Kang, E. Reichmanis, *Angew. Chem. Int. Ed.* **2012**, *51*, 11841.
[44] A. Monguzzi, M. Frigoli, C. Larpent, R. Tubino, F. Meinardi, *Adv. Funct. Mater.* **2012**, *22*, 139.
[45] Y. C. Simon, C. Weder, *J. Mater. Chem.* **2012**, *22*, 20817.
[46] C. Wohnhaas, A. Turshatov, V. Mailänder, S. Lorenz, S. Baluschev, T. Miteva, K. Landfester, *Macromol. Biosci.* **2011**, *11*, 772.
[47] M. Sitkovsky, D. Lukashev, *Nat. Rev. Immunol.* **2005**, *5*, 712.
[48] S. M. Borisov, C. Larndorfer, I. Klimant, *Adv. Funct. Mater.* **2012**, *22*, 4360.
[49] R. A. Petros, J. M. DeSimone, *Drug Discovery* **2010**, *9*, 615.
[50] A. Monguzzi, R. Tubino, F. Meinardi, *Phys. Rev. B* **2008**, *77*, 155122.
[51] I. Berlman, *Handbook of florescence spectra of Aromatic Molecules*; 2nd ed.; New York, 2012.
[52] S. M. Borisov, G. Zenkl, I. Klimant, *ACS Appl. Mater. Interfaces* **2010**, *2*, 366.
[53] T. Ogawa, N. Yanai, A. Monguzzi, N. Kimizuka, *Sci. Rep.* **2015**, *5*, 10882.
[54] A. Monguzzi, R. Tubino, S. Hoseinkhani, M. Campione, F. Meinardi, *Phys. Chem. Chem. Phys.* **2012**, *14*, 4322.
[55] D. B. Papkovsky, T. C. O'Riordan, *J. Fluoresc.* **2005**, *15*, 569.

[56] A. Monguzzi, R. Tubino, M. M. Salamone, F. Meinardi, *Phys. Rev. B* **2010**, *82*, 125113.
[57] C. Y. Tay, Y. Yu, M. I. Setyawati, J. Xie, D. T. Leong, *Nano Res.* **2014**, *7*, 805.
[58] A. Manke, L. Wang, Y. Rojanasakul, *Biomed. Res. Int.* **2013**, *2013*, 942916.

Received: ((will be filled in by the editorial staff))
Revised: ((will be filled in by the editorial staff))
Published online: ((will be filled in by the editorial staff))

The use of the well-known Kolliphor EL surfactant enables the preparation of stable micelles loaded with a sensitizer/emitter couple showing efficient Triplet-Triplet Up Conversion emission in oxygenated environment. Such micelles can be used as anti-Stokes fluorescent probes in the staining of 3T3 stem cells paving the way for low excitation power imaging within living tissues.

Keyword: fluorescence imaging, triplet-triplet annihilation, up conversion, Kolliphor EL, micelles

Sara Mattiello, Angelo Monguzzi, Jacopo Pedrini, Mauro Sassi, Chiara Villa, Yvan Torrente, Roberto Marotta, Francesco Meinardi, and Luca Beverina*

Self-assembled dual dye-doped nanosized micelles for high-contrast up-conversion bioimaging

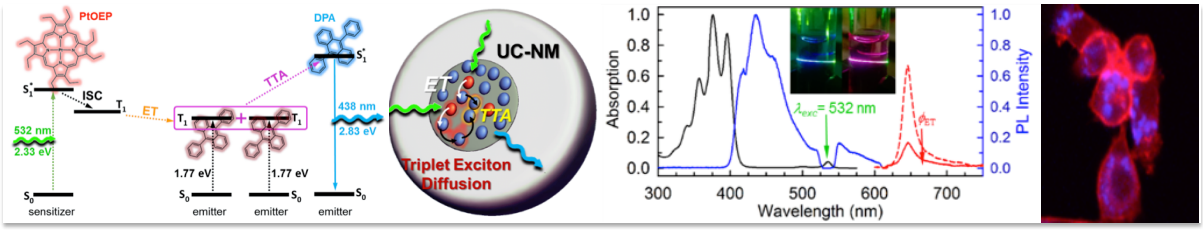

Copyright WILEY-VCH Verlag GmbH & Co. KGaA, 69469 Weinheim, Germany, 2013.

Supporting Information

Self-assembled dual dye-doped nanosized micelles for high-contrast up-conversion bioimaging.

By *Sara Mattiello, Angelo Monguzzi, Jacopo Pedrini, Mauro Sassi, Chiara Villa, Yvan Torrente, Roberto Marotta, Francesco Meinardi and Luca Beverina*

1. Figure S1.

Figure S1. Digital picture of the aqueous PBS dispersion of dual dye-doped up-converting nanomicelles (UC-NMs) obtained by the synthesis protocol described in the main text.

2. Figure S2.

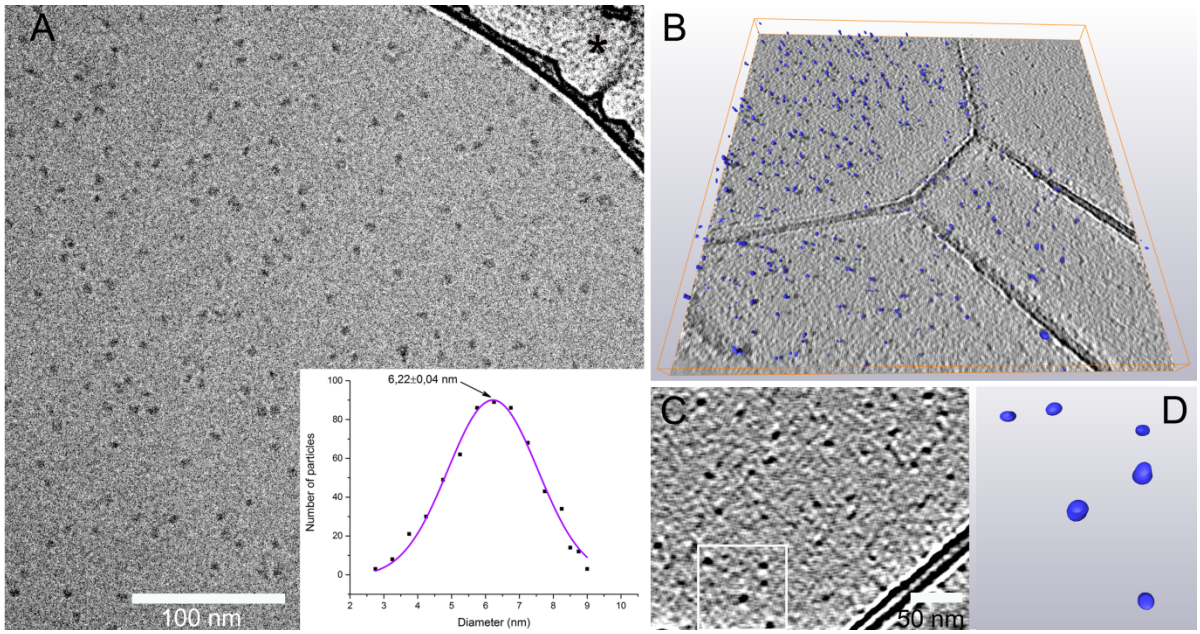

Figure S2. Cryo-TEM of Kolliphor micelles loaded with a PtOEP:DPA 1:100 cargo. A, projection image of micelles in their fully hydrated state. The asterisk points to the grid carbon membrane. Inset: graph showing the particles diameter statistical analysis. B, 3D model of the micelles (in blue) in their vitrified solution representing the reconstruction of a cryo-electron tomogram acquired at low electron dose (see Supplemental Movie S1). The 3D model is set on a single tomographic slice. C, averaged single tomographic slice of the tomogram in B. D, 3D model of the micelles boxed in C.

3. Figure S3

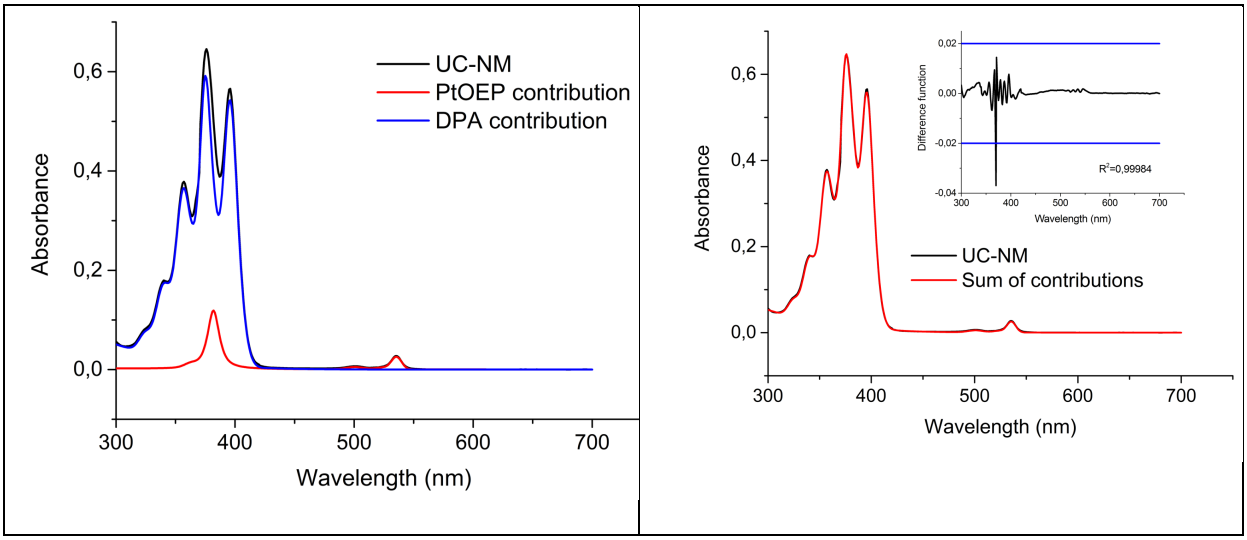

Figure S3. Left: UV-Vis absorption of UC-NMs (black, water dispersion). The spectrum can be deconvoluted separating the contribution of DPA (blue) and PtOEP (red), respectively. By comparing the molar extinction coefficient of the dyes, we estimate that in the dispersion the PtOEP:DPA concentration ratio is 1:96, accordingly with the initial 1:100 feeding ration used in the synthesis. Right: comparison between the micellar solution absorption and the linear combination of the two distinct DPA and PtOEP contributions obtained according to the feeding ratio. The inset shows the difference function between experimental and calculated values.

4. Figure S4.

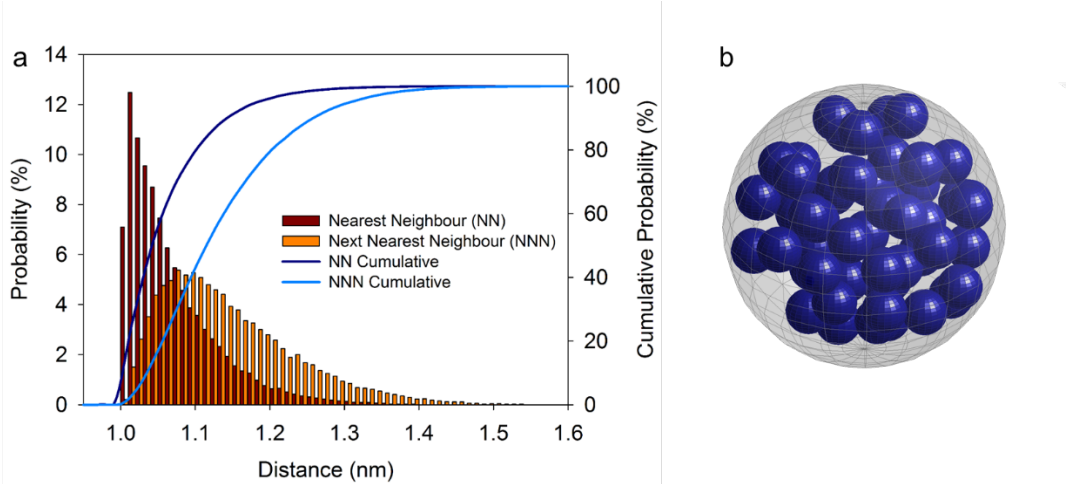

Figure S4. (a) Histogram of the intermolecular stochastic nearest-neighbor (NN) and next nearest-neighbor (NNN) distance distribution of an ensemble of 56 DPA molecules embedded in a spherical UC-NM of radius 6.2 nm. The continuous line are the corresponding cumulative probabilities. (b) One example of the 10^5 randomly generated distributions.
56 is the average number of DPA molecules in a micelle, calculated as the ratio of the total number of DPA molecules to the estimated number of micelles. The number of micelles is calculated as the ratio of the total volume of Kolliphor EL® (0.15 cm3) to the average volume of a single micelle, based on the diameter obtained from DLS measurements (15 nm).

5. Figure S5.

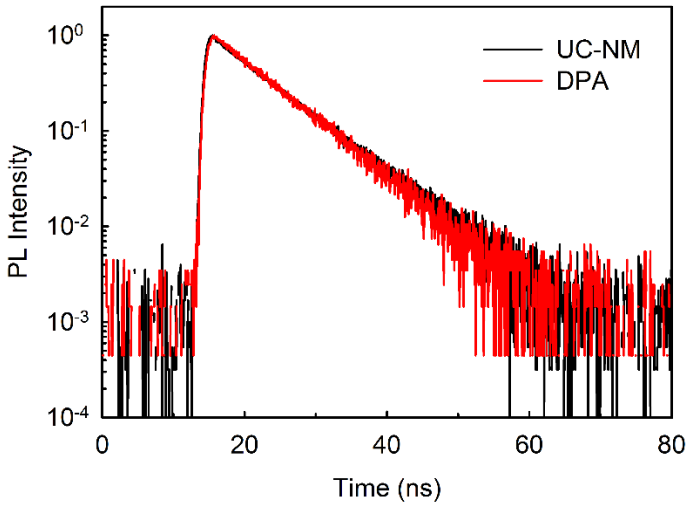

Figure S5. Time resolved fluorescence of UC-NM (black) and DPA (10^{-6} M, THF solution) under pulsed excitation at 340 nm.

6. Figure S6

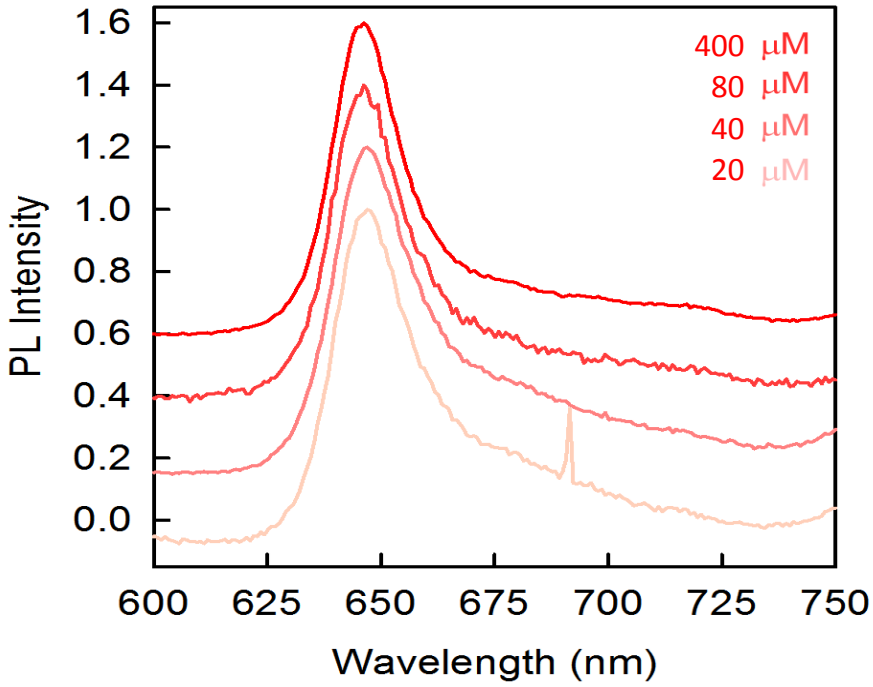

Figure S6. Normalized PL spectrum of nanomicelles prepared with different PtOEP initial concentration under 532 nm CW laser excitation.

7. Figure S7

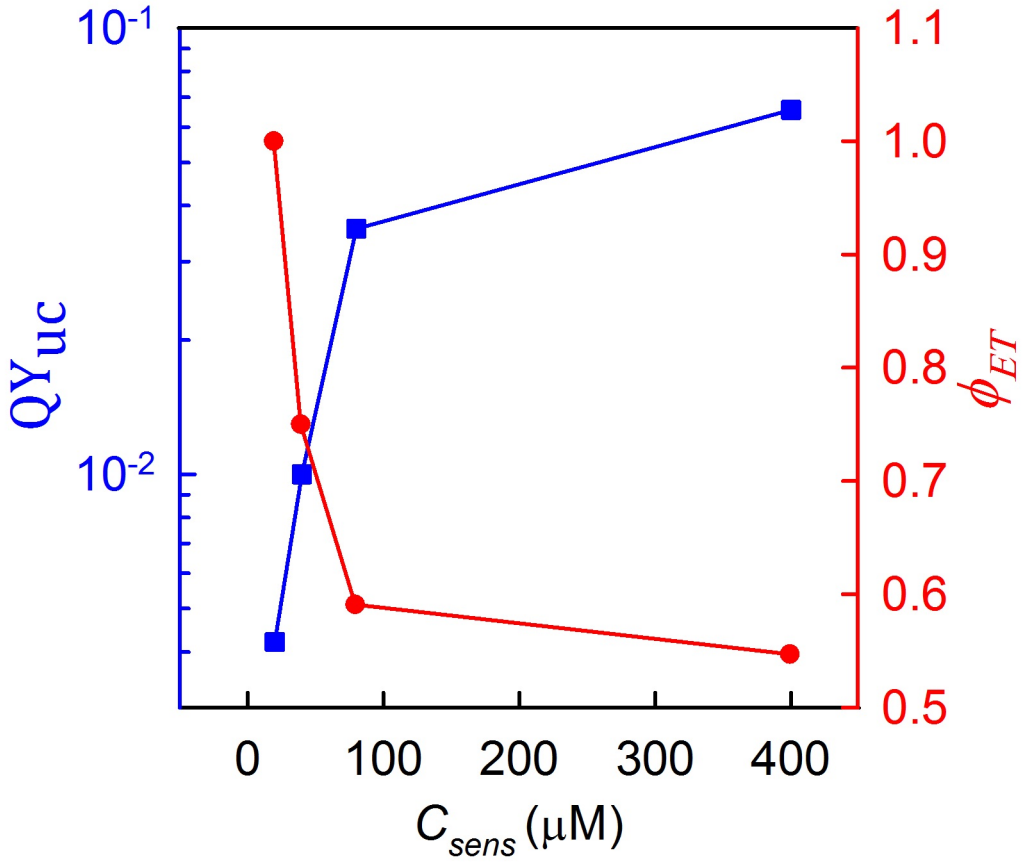

Figure S7. QY_{uc} and ϕ_{ET} measured for a series of UC-NM prepared with a fixed DPA initial concentration (400 μM) as a function of C_{sens}.

8. Figure S8.

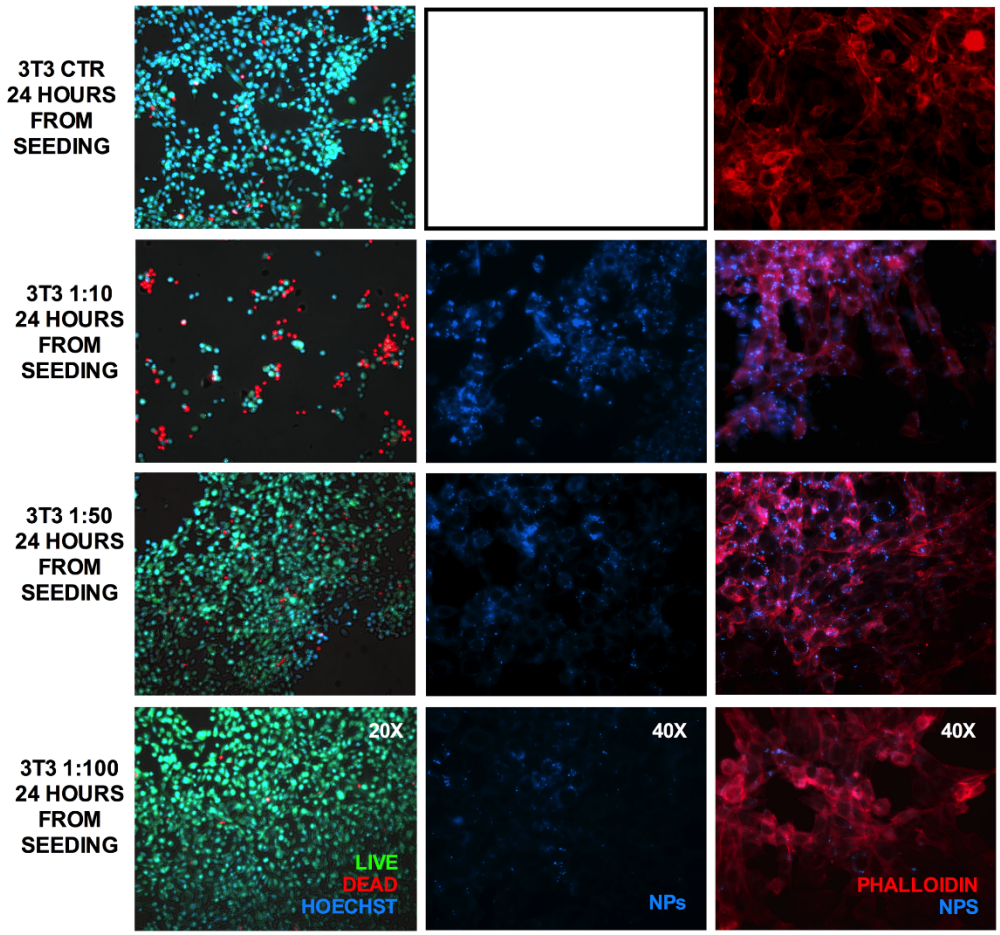

Figure S8. (left) Live/Dead test results on 3T3 fibroblast stem cells stained with Hoechst (center) Fluorescence imaging of 3T3 cells stained with UC-NMs under UV excitation. (right) Fluorescence imaging of 3T3 cells stained with UC-NMs (blue) and phalloidin under UV excitation.

9. Details on photophysical measurements.

Energy Transfer Efficiency Measurements.

The sensitizer-to-emitter ET efficiency (ϕ_{ET}) has been calculated from the measurements of the sensitizer residual PL in presence (I) and in absence (I_0) of the emitter as [1]

$$\phi_{ET} = = 1\text{-}I/I_0 . \qquad \text{Eq. S1}$$

TTA-UC Quantum Yield Measurements.

The up-conversion luminescence quantum efficiency of polymeric up-converters was determined by comparison with a DPA-PtOEP UC pair in deaerated tetrahydrofuran ([DPA] = 10 mM, [PtOEP] = 100 μM) used as secondary standard, according to the following equation

$$QY_{uc} = QY_{std}\left(\frac{A_{std}}{A_{uc}}\right)\left(\frac{I_{uc}}{I_{std}}\right)\left(\frac{P_{std}}{P_{uc}}\right)\left(\frac{\eta_{uc}}{\eta_{std}}\right)^2 \qquad \text{Eq. S2}$$

where QY, A, I, P and η represent quantum yield, absorptance at excitation intensity, integrated photoluminescence spectral profile, excitation power density, and refractive index of the medium. The subscripts "*std*" and "uc" indicate the reference and the sample, respectively. The UC quantum yield of the secondary standard is 0.24 at its maximum[2].[4] The recorded spectra have been corrected for the setup optical response. The refraction index of tetrahydrofuran is 1.41 at 293 K and 1.33 for water.The secondary standard solution is freshly prepared and characterized before each run of measurements. It should be noted that in the high excitation power density limit the QY_{uc} does not depend on the excitation intensity. The sample have been measured in a 1 mm optical path cuvette, the same used for the solution sample. The used setup works in a collinear geometry, which is insensitive to the position in which the photoluminescence is generated, enabling us to compare also samples with different absorbance without incurring in trivial errors.

10. Figure S9.

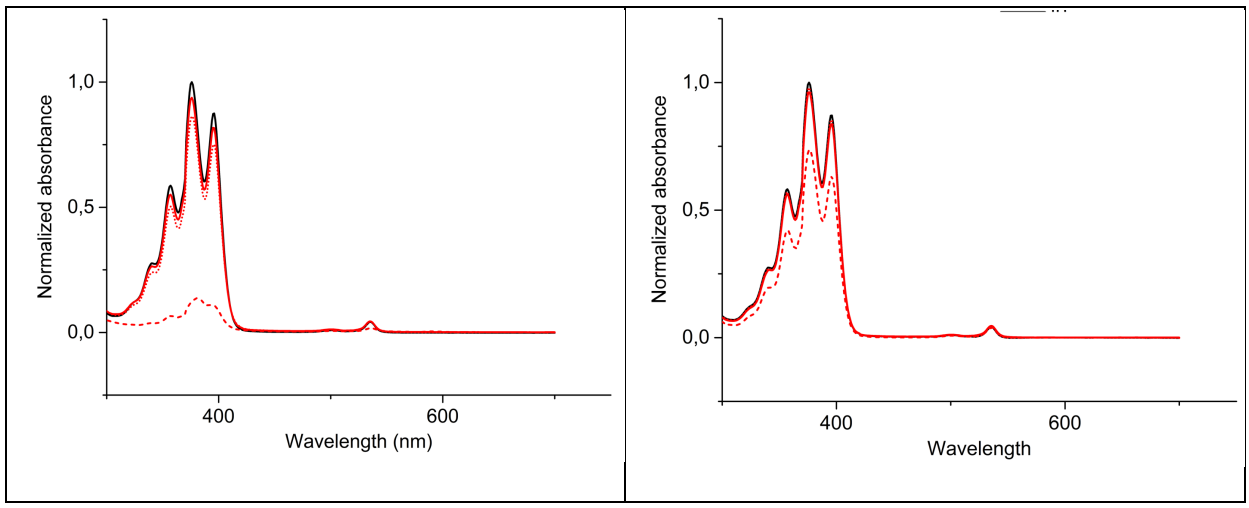

Figure S9. Left: UV-Vis absorption of UC-NMs kept under sunlight immediately after preparation (black line), 1 day after preparation (red, full line), 2 days after preparation (red, dotted line) and 15 days after preparation (red, dashed line). Right: UV-Vis absorption of UC-NMs kept at 4°C in the dark immediately after preparation (black line), 1 day after preparation (red, full line), 2 days after preparation (red, dotted line) and 15 days after preparation (red, dashed line).

11. References for the Supporting Information section.

[1] M. Inokuti, F. Hirayama, The Journal of Chemical Physics 1965, 43, 1978.
[2] A. Monguzzi, R. Tubino, S. Hoseinkhani, M. Campione, F. Meinardi, Physical Chemistry Chemical Physics 2012, 14, 4322.